

# Operando UV/vis Spectroscopy Providing Insights into the Sulfur and Polysulfide Dissolution in Magnesium–Sulfur Batteries

Joachim Häcker,\* Duc Hien Nguyen, Tobias Rommel, Zhirong Zhao-Karger, Norbert Wagner, and K. Andreas Friedrich

Cite This: *ACS Energy Lett.* 2022, 7, 1–9

Read Online

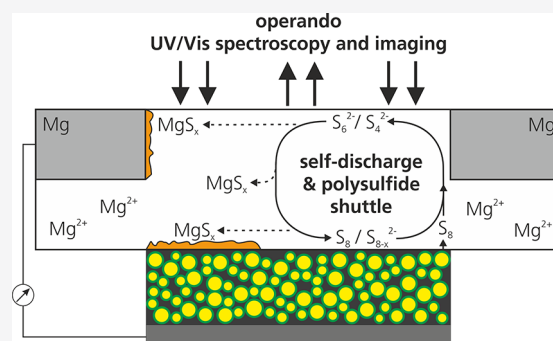
ACCESS |

Metrics & More

Article Recommendations

Supporting Information

**ABSTRACT:** The magnesium–sulfur battery represents a promising post-lithium system with potentially high energy density and improved safety. However, just as all metal–sulfur systems, it is plagued with the polysulfide shuttle leading to active material loss and surface layer formation on the anode. To gain further insights, the present study aims to shed light on the dissolution characteristics of sulfur and polysulfides in glyme-based electrolytes for magnesium–sulfur batteries. Therefore, operando UV/vis spectroscopy and imaging were applied to survey their concentration in solution and the separator coloration during galvanostatic cycling. The influence of conductive cathode additives (carbon black and titanium nitride) on the sulfur retention and cycling overpotentials were investigated. Thus, valuable insights into the system's reversibility and the benefit of additional reaction sites are gained. On the basis of these findings, a reduction pathway is proposed with  $S_8$ ,  $S_6^{2-}$ , and  $S_4^{2-}$  being the present species in the electrolyte, while the dissolution of  $S_8^{2-}$  and  $S_3^{2-}$  is unfavored. In addition, the evolution of the sulfur species concentration during an extended rest at open-circuit voltage was investigated, which revealed a three-staged self-discharge.



In the past decade, there has been increasing interest in post-lithium-ion batteries. Among others, the electrochemical couple of magnesium and sulfur is a promising candidate and under intensive research as a sustainable high-energy battery system. Indeed, its high theoretical energy density of  $2400 \text{ Wh L}^{-1}$  and  $1330 \text{ Wh kg}^{-1}$  is significantly decreased when considering a realistic cell setup; thus, Mg–S cells might not be able to compete with Li-ion and Li–S batteries in terms of volumetric and gravimetric energy densities, respectively.<sup>1</sup> However, in contrast to other metal anodes such as Li, Na, K, Ca, or Al, magnesium offers a lower tendency for dendrite formation and therefore improved safety during cycling.<sup>2</sup> Furthermore, due to its abundance, it represents a cost-effective, sustainable, and easily recyclable battery alternative.

Mechanistic studies of Mg–S cells revealed that the electrochemical reaction is comparable to lithium–sulfur batteries, namely, the reduction from elemental sulfur to a solid product with  $MgS_x$  species as intermediates.<sup>3,4,5</sup> Their solubility enhances the redox reactions due to faster liquid-phase reaction kinetics, but on the other hand the well-known issues of self-discharge, polysulfide shuttle, overcharge, and active material loss arise. Because sulfur species feature

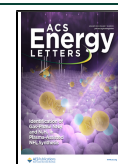
absorption in the visible light spectrum and consequently cause a coloration of the electrolyte and separator, UV/vis spectroscopy is a well-suited method to investigate their dissolution behavior. Previous studies took advantage and applied this technique to ex situ<sup>6,7</sup> and operando studies of Li–S batteries in transmission<sup>8,9</sup> and reflection mode.<sup>10,11</sup> Interesting insights are gained by Zou et al., as they highlight the significant influence of the electrolyte solvent on the redox reactions.<sup>9</sup>

In recent years, UV/vis spectroscopy was also utilized to investigate Mg–S cells, starting with ex situ investigations at selected cycling stages.<sup>3,12</sup> A systematic analysis of  $MgS_x$  species in different solvents<sup>13</sup> and electrolytes<sup>14</sup> was conducted by Bieker et al., which unveiled significant differences in the disproportionation/dissociation behavior of lithium and

Received: October 3, 2021

Accepted: November 5, 2021

Published: November 19, 2021



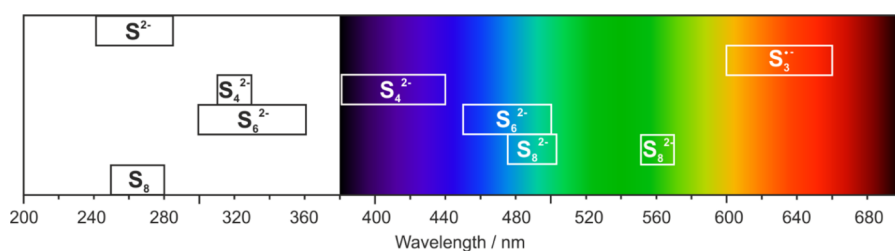


Figure 1. Sulfur species ( $S_8$ ,  $S_8^{2-}$ ,  $S_6^{2-}$ ,  $S_4^{2-}$ ,  $S_3^{\bullet-}$ , and  $S^{2-}$ ) and their main corresponding absorption region in the ultraviolet and visible light spectrum on the basis of previous studies on different metal polysulfides (Table S1).

magnesium polysulfides solutions. It was found that the currently used electrolyte solvents for Mg–S cells, namely, glymes and ethers, hardly stabilize short-chain polysulfides such as  $S_4^{2-}$  and  $S_3^{\bullet-}$ , which might be the origin of large overpotentials during reduction to magnesium sulfide and their subsequent reoxidation. Drvarič Talian et al. adopted this approach to synthesize distinct  $MgS_x$  ( $x = 4, 6, 8$ ) solutions and study their disproportionation and redox kinetics in situ.<sup>15</sup> Recently, an extensive ex situ study by Ford et al. highlighted the importance of self-discharge and found it to be severe in all common magnesium electrolytes.<sup>16</sup> However, to the best of our knowledge, there is a lack of systematic operando studies of Mg–S cells to ascertain the cycling and self-discharge properties as ex situ measurements suffer from possible changes of the  $MgS_x$  species and concentration. Therefore, the present study aims to directly investigate the  $MgS_x$  evolution during cycling and extended rest at open-circuit voltage (OCV) to assess the cell's reversibility and self-discharge, respectively.

## GALVANOSTATIC CYCLING

As previously demonstrated for the Li–S system,<sup>10</sup> the absorbance can be calculated from the continuously collected transmission UV/vis spectra by applying the Lambert–Beer law. To consider possible changes in the spectra, which are not caused by polysulfide absorbance, namely, slight shifts in the lamp spectrum or drying of the separator, the spectra are normalized. Experimental details are depicted in the Supporting Information.

For the UV/vis spectra analysis, specific wavelengths at the absorbance maxima are identified and subsequently correlated to sulfur species on the basis of previous literature on sulfur and metal polysulfides (Figure 1 and Supporting Information Table S1).<sup>3,6,7,9,13</sup> Because the distinct absorbance energy is solvent-dependent, the specific wavelengths slightly vary when applying other electrolyte systems. Despite the polysulfide solubility being cation-dictated,<sup>13</sup> the actual region of the absorbance, however, hardly differs from lithium to magnesium polysulfides, as cations and polysulfide anions are dissociated in solution. The fact that some polysulfide anions ( $S_8^{2-}$ ,  $S_6^{2-}$ , and  $S_4^{2-}$ ) absorb light at two different wavelength regions might be originated in their solvation shell, i.e., the number of coordinating solvent molecules.

Exemplary UV/vis spectra at characteristic cycling stages of a Mg–S cell (Figure S8) are plotted in Figure 2. The initial spectra are similar to previously reported data,<sup>13</sup> with the spectra being dominated by absorbance peaks at 237 and 280 nm, which can be assigned to elemental sulfur ( $S_8$ ) dissolved in the electrolyte. Furthermore, a small shoulder at 410 nm, corresponding to the short-chain polysulfide  $S_4^{2-}$ , is already present after cell assembly. Interestingly, this peak intensifies in

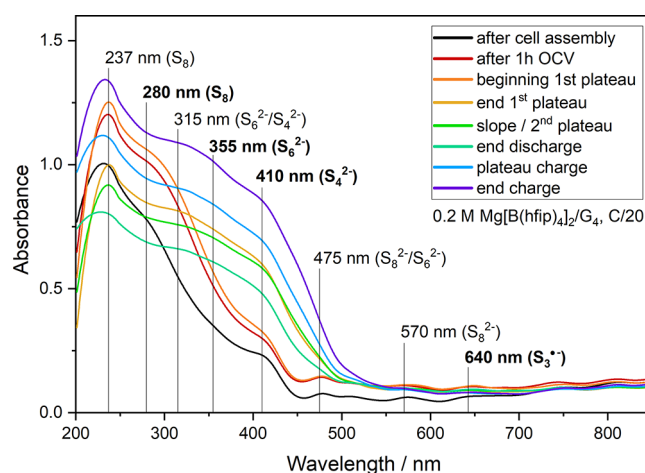


Figure 2. Exemplary UV/vis spectra collected at different C/20 cycling stages of a Mg/S cell comprising a 0.2 M  $Mg[B(hfp)_4]_2/G_4$  electrolyte and a S/KB/CMC-SBR (50/40/10 wt %) cathode. The corresponding potential curve is depicted in Figure S8. Absorbance peaks are indicated and correlated to sulfur species identified in previous studies.

the subsequent discharge, which is in strong contrast to the findings by Bieker et al., where hardly no  $S_4^{2-}$  was detected in glyme-based solutions and electrolytes.<sup>13,14</sup> These results further support the fact that the involved cation—Li<sup>+</sup> or Mg<sup>2+</sup>—plays a crucial role in the stability and solubility of polysulfides. In case of magnesium,  $S_6^{2-}$  and  $S_4^{2-}$  species are easily synthesizable in glymes electrochemically, while their chemical synthesis takes far more effort than their lithium counterparts. Therein, stoichiometric mixing of  $Li_2S$  and  $S_8$  in solution is sufficient and rather defined solutions with high  $Li_2S_x$  concentrations (>1 M) are synthesizable,<sup>17</sup> whereas the preparation of  $MgS_x$  solutions requires high-energy ball-milling<sup>18</sup> or the presence of complexing agents<sup>9</sup> and magnesium salts.<sup>16</sup>

While  $S_8^{2-}$  species with their absorption being reported in the region of 475–505 and 560 nm were not detected, two peaks at 315 and 355 nm are present. The latter is assigned to  $S_6^{2-}$ , which is further backed by a small shoulder at 475 nm. A distinct assignment of the peak at 315 nm is hampered due to overlap of absorption wavelengths of  $S_6^{2-}$  and  $S_4^{2-}$  and was therefore not considered in the subsequent analysis. The polysulfide radical  $S_3^{\bullet-}$  (640 nm) was not detected at all, which is in agreement with Bieker et al.<sup>13,14</sup> and relates to the strong interaction of  $Mg^{2+}$  with polysulfide species in glymes, which favors the reduction or disproportionation to high charge density polysulfides such as  $S_4^{2-}$ .

To survey the evolution of specific sulfur species ( $S_8$ ,  $S_6^{2-}$ ,  $S_4^{2-}$ , and  $S_3^{\bullet-}$ ), their corresponding wavelengths (280, 355,

410, and 640 nm) are plotted together with the voltage profile over time in Figure 3. In addition, the operando images of the separator at characteristic stages are depicted below.

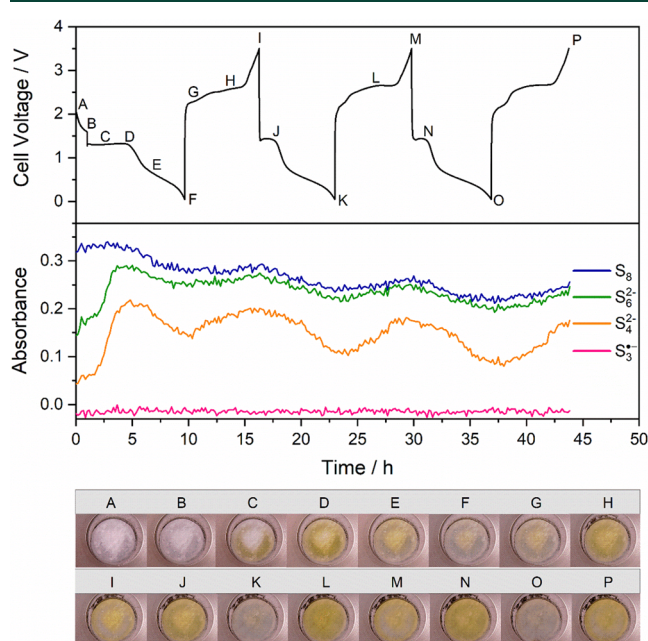
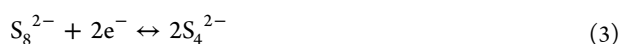
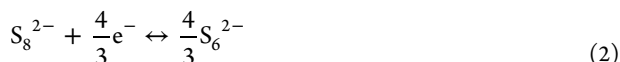


**Figure 3.** Voltage profile, absorbance and images of operando optical cells cycled at C/20 comprising a 0.2 M Mg[B(hfp)<sub>4</sub>]<sub>2</sub>/G4 electrolyte and a S/KB/CMC-SBR (50/40/10 wt %) cathode.

The already high concentration of elemental sulfur after cell assembly (A) reflects the fast diffusion of S<sub>8</sub> in the electrolyte accompanied by a drop in cell voltage. Simultaneously to S<sub>8</sub>, the concentration of S<sub>6</sub><sup>2-</sup> and S<sub>4</sub><sup>2-</sup> species during the initial 1 h OCV increases (B). In our previous study,<sup>20</sup> we assumed this to be originated in elemental sulfur being partially reduced to S<sub>8</sub><sup>2-</sup> at the anode via the following non-faradaic reaction:



The other option, namely, the reaction of elemental sulfur with electrolyte at the cathode side, was excluded by Ford et al., who ascertained, using UPLC-MS, that the presence of Mg metal is required for the self-discharge to be initiated.<sup>16</sup> This was confirmed as the separator in a Mg anode-free cell stays uncolored during extended rest (Figure S15). Because S<sub>8</sub><sup>2-</sup> is not detected, an instant subsequent reaction to S<sub>6</sub><sup>2-</sup>/S<sub>4</sub><sup>2-</sup> has to take place—either further via non-faradaic reaction at the anode,



or via chemical reaction, i.e., disproportionation,



The preferred reaction mainly depends on the electrolyte's solubility limit. In an electrolyte with higher solubility limit, the formed polysulfides might diffuse away from the Mg surface,

where instant disproportionation has to take place to exclude S<sub>8</sub><sup>2-</sup> detection. Assuming a sulfur species concentration already close to the solubility limit, ongoing non-faradaic reaction with Mg metal is likely. A distinct interpretation is difficult, but at least it can be concluded that either one of these reactions must possess fast kinetics. The direct reduction of S<sub>8</sub> to form two S<sub>4</sub><sup>2-</sup> molecules without any S<sub>8</sub><sup>2-</sup> intermediate is assumed to be unlikely due to the large number of concurrently transferred electrons in a single step.

During the first discharge plateau (C, D), the desired faradaic reaction at the cathode side, namely, the reduction of elemental sulfur to S<sub>6</sub><sup>2-</sup> and S<sub>4</sub><sup>2-</sup>, takes place (eqs 1–3). Due to their solubility in the electrolyte, they diffuse into the separator, causing its bright yellow coloration (D). With proceeding discharge (E, F), the overall concentration of sulfur species in the electrolyte decreases to end up with an only partially colored separator (F). This indicates that there is a strong driving force for the polysulfides to diffuse back to a conductive carbon surface to be further reduced on the cathode side, potentially via the following reactions:



However, the still rather high concentrations of S<sub>8</sub>, S<sub>6</sub><sup>2-</sup> and S<sub>4</sub><sup>2-</sup> at the end of the discharge show the severe loss of active material due to its inaccessibility in the separator.

During charge, the reoxidation of (poly-)sulfides leads to an increase of the S<sub>4</sub><sup>2-</sup>, S<sub>6</sub><sup>2-</sup>, and S<sub>8</sub> concentration in the electrolyte (G, H), but despite a high-charge-cutoff potential, there is no decline in concentration toward the end of charge (I)—not even for the short-chain polysulfide S<sub>4</sub><sup>2-</sup>. This indicates an incomplete reoxidation of the dissolved sulfur species to elemental sulfur and a capacity loss during charging. This becomes noticeable in a shorter first plateau in the subsequent discharge (J). This undulatory trend, i.e. the increase and decrease in concentration, repeats in the following cycles with constant amplitude (Figure S7) and is qualitatively reproducible (Figure S8).

## ■ CATHODE ADDITIVES

Among the sulfur retention approaches, the incorporation of polar additives in the cathode structure is rather popular. Compounds featuring intrinsic electrical conductivity are of special interest as they not only adsorb the sulfur species but may directly act as reaction sites. For this purpose, along with conductive carbon black (C-ENERGY Super C45), titanium nitride (TiN) was chosen in this study (Table S2). To ensure comparability, powders with a similar specific surface area of 45 and 48 m<sup>2</sup>/g for C45 and TiN, respectively, were selected and the weight ratio in the cathode composition (10 wt %) as well as the sulfur loading (1 mg/cm<sup>2</sup>) was kept constant.

The corresponding plots of voltage and absorbance over time are depicted in Figures 4 and 5. Therein, the overall absorbance value is comparable to the standard cathode (Figure 3), which reflects a similar sulfur/polysulfide concentration in the electrolyte and indicates no beneficial retention effect. Despite attention being paid to an identical cell assembly, the electrode and separator positioning slightly differs for each cell. Thus, differences in intensity between cells might arise, which hinder the quantitative comparison of the gained absorbance values. Furthermore, the synthesis of complexing agent-free distinct magnesium polysulfide solutions

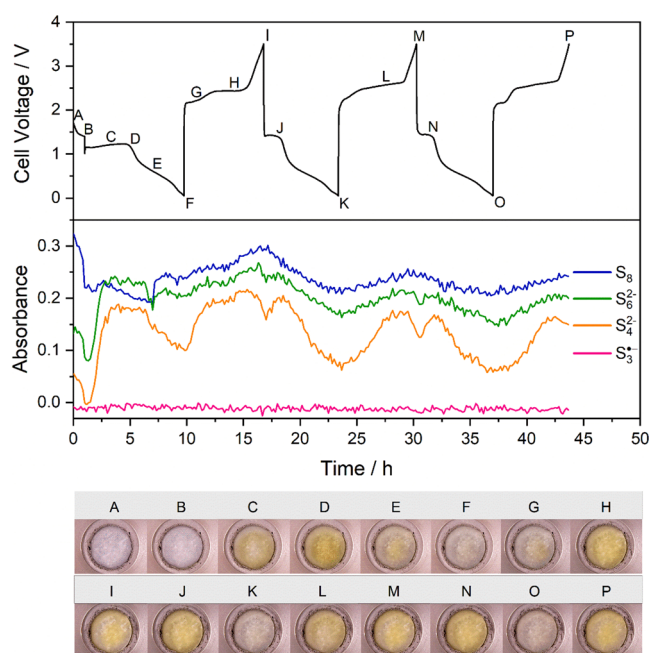


**Figure 4.** Voltage profile, absorbance, and images of operando optical cells cycled at C/20 comprising a 0.2 M  $\text{Mg}[\text{B}(\text{hfp})_4]_2/\text{G4}$  electrolyte and a S/KB/C45/CMC-SBR (44.4/35.6/10/10 wt %) cathode.

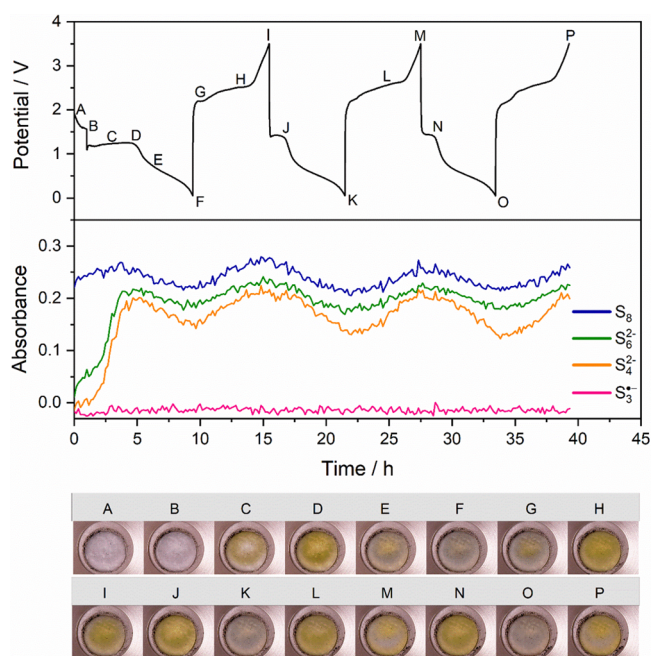


**Figure 5.** Voltage profile, absorbance, and images of operando optical cells cycled at C/20 comprising a 0.2 M  $\text{Mg}[\text{B}(\text{hfp})_4]_2/\text{G4}$  electrolyte and a S/KB/TiN/CMC-SBR (44.4/35.6/10/10 wt %) cathode.

with defined concentration as reference solutions is hardly possible. Therefore, the discussion only focuses on the present species, their relative absorbance values in a single measurement, and the comparison of their qualitative trend between different measurements.

Herein, after an initial drop in concentration, a similar trend during the first discharge, namely, a strong increase of  $\text{S}_6^{2-}$  and  $\text{S}_4^{2-}$  in the first plateau is observed. However, during charge

the absorbance differs for the C45-containing cathode (Figure 4) with the  $\text{S}_4^{2-}/\text{S}_6^{2-}$  concentration in the electrolyte being reduced toward the charge-cutoff potential. This might originate from a larger number of reaction sites which enables a faster reoxidation of short-chain polysulfides during charge. In contrast, cathodes with TiN (Figure 5) do not feature such decline in polysulfide concentration—despite proving to be suitable as an adsorption center/redox mediator in Li–S batteries ( $\text{TiN}^{21-26}$ ). Because the surface areas of C45 ( $45 \text{ m}^2/\text{g}$ ) and TiN ( $48 \text{ m}^2/\text{g}$ ) are very similar, the different behavior is either linked to the higher electrical conductivity of C45 vs TiN (1.77 vs  $0.024 \text{ S}/\text{cm}$ , Table S2) or originated in a higher tendency for polysulfides to adsorb at the carbon surface. This points to the reaction being charge-transfer—rather than mass-transport-limited. The adsorption energy can indeed be estimated by density functional theory (DFT), which goes beyond the scope of this work, but should be part of subsequent studies.

As mentioned above, the trend during the initial 1 h OCV differs for the C45-cathode, with the sulfur and polysulfide concentrations in the electrolyte steadily decreasing. However, this was not interpreted further as—in contrast to the declining polysulfide concentration toward charge cutoff—this could not be reproduced (Figure S13) and might stem from spectra deviations in the initial wetting process compared to the reference measurement.

Despite the decay in  $\text{S}_4^{2-}/\text{S}_6^{2-}$  concentration during charge of the C45-cathode, the separator still exhibits a yellowish coloration (I) similar to Figure 3 and in contrast to the almost colorless separator at the end of discharge (F). Indeed, the decline in concentration of  $\text{S}_6^{2-}$  species during discharge follows  $\text{S}_8$  rather than  $\text{S}_4^{2-}$  species, however, during charge the concentration trend of  $\text{S}_4^{2-}$  and  $\text{S}_6^{2-}$  concentrations is rather similar (especially in Figure S13). This is in contrast to previous reports in the Li–S system, where  $\text{S}_6^{2-}$  is consumed while the  $\text{S}_4^{2-}$  concentration rises—and vice versa.<sup>8</sup> Their equilibrium can be defined by the electrochemical reaction:



and the chemical reaction, i.e., disproportionation,



As depicted in eq 6,  $\text{S}_4^{2-}$  might be a crucial intermediate toward the solid product at the end of discharge. If the  $\text{S}_2^{2-}/\text{S}^{2-}$  formation occurs at the expense of  $\text{S}_4^{2-}$  species, the equilibrium in eq 8 is altered and the  $\text{S}_6^{2-}$  concentration should be declining similarly. However, in Figures 3–5 and S13, it is only declining moderately during discharge, suggesting that the reduction kinetics are rather slow. Considering that concentration trend, the disproportionation eq 9 is unfavored, whereas the liquid–solid transition could take place via disproportionation eq 10. However, the concentration of  $\text{S}_4^{2-}$  (and  $\text{S}_6^{2-}$ ) during extended OCV appears to be very stable (Figures 8 and S14), why the disproportionation eqs 9 and 10 are both considered unlikely.

In Figure 6, a reduction pathway is proposed summarizing the previously gained insights. In general, the equilibrium of the sulfur species depends on temperature, concentration, and solvent properties. In solvents with high dielectric permittivity

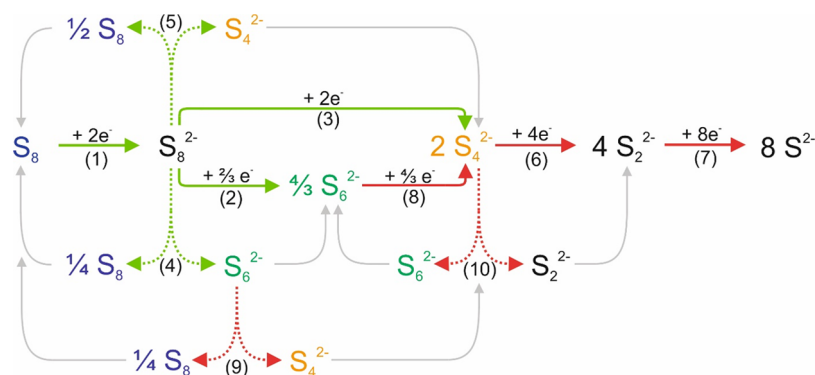


Figure 6. Proposed reduction pathway for sulfur species in glyme-based electrolytes. Solid and dashed lines represent electrochemical and chemical reactions (disproportionation), respectively. Reactions with fast and sluggish kinetics are marked in green and red, respectively, and are labeled with the equation numbers in the text. Note that only information about the species in the electrolyte/separator are gained, and the distinct composition of the solid compounds is unknown.

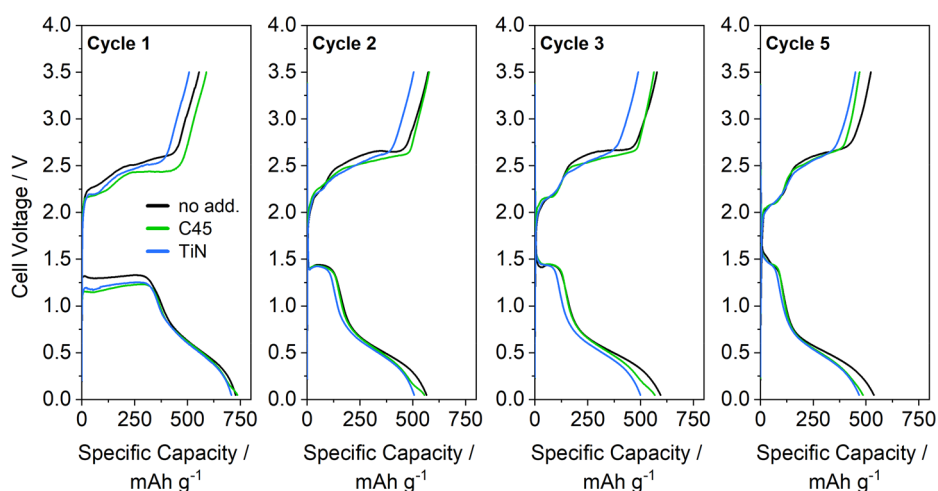


Figure 7. Influence of conductive additives (10 wt % C45 or TiN) on the potential plateaus and overpotentials arising during galvanostatic cycling at C/20.

and donor number (e.g., DMSO, DMF, or ACN) the low charge density polysulfides  $S_8^{2-}$ ,  $S_6^{2-}$ , and  $S_3^{\bullet-}$  are dominant, while in solvents with low dielectric permittivity and donor number (G1, G2, G4, THF) the high charge density polysulfide  $S_4^{2-}$  is well-stabilized.<sup>13,14</sup> It should be kept in mind that the pathway in Figure 6 relies on the observed polysulfides in solution, not at the cathode side. It is further noted that the liquid–solid reaction of  $S_4^{2-}$  to  $S_2^{2-}/S^{2-}$  at the cathode is just an assumption and the composition of the solid compounds is unknown. In fact, there is a disagreement in literature stating  $MgS_2$ <sup>12,27</sup> or  $Mg_3S_8$ <sup>28</sup> as intermediate, while others did not observe any intermediate.<sup>4,5</sup>

Comparing the potential plateaus and gained capacities of the cells comprising no additive and cells with 10 wt % TiN and C45 (Figure 7) only minor differences are observed. In the initial cycle, the additives—especially C45—are beneficial in reducing the charge potential of the first and second plateaus from 2.3 to 2.2 V and from 2.6 to 2.45 V, respectively. The corresponding  $S_8$ ,  $S_6^{2-}$ , and  $S_4^{2-}$  concentrations in Figures 3–5 increase concurrently during charge—the latter to a larger extent due to  $S_4^{2-}$  being the initial soluble intermediate. While the first charge plateau can be assigned to the reaction from solid to liquid phase ( $S^{2-}/S_2^{2-}$  to  $S_4^{2-}$ , eq 6), the second plateau correlates with the reaction from liquid to solid phase ( $S_4^{2-}$  to  $S_8$ ). However, an unambiguous assignment of the

underlying reaction pathway in the second plateau is difficult. As the  $S_6^{2-}$  concentration rises simultaneously to  $S_8$ , the oxidation of  $S_4^{2-}$  is assumed to partially take place via eq 3 + 1 and 8 + 2 + 1. In case of the C45-cathode, simultaneous depletion of  $S_6^{2-}$  and  $S_4^{2-}$  in the electrolyte appears (Figure S13)—however only after the second plateau—resulting in an increase in overpotential due to insulating elemental sulfur blocking conductive sites and the solid state diffusion of magnesium ions being rather slow. Severe polysulfide shuttling, i.e., the ongoing reduction of long-chain polysulfides or elemental sulfur at the anode was not observed.

In the corresponding images, the formation of black deposits on the anode surface are detected during charge at approximately 2.5 V (Figures 3–5H and Figure 8I). This might originate from sulfide precipitation or electrolyte decomposition at the anode. The electrolyte salt exhibits a high oxidative stability of 3.5 V on Al and stainless steel;<sup>18</sup> however, its stability appears to be lower on Mg as indeed fluoride species from the electrolyte salt were found to contribute to the SEI formation on the Mg surface in previous studies.<sup>20</sup> Furthermore, the precipitation of sulfur species such as  $MgS$ ,  $MgSO_4$ ,<sup>20</sup> or  $MgS_{6-8}$ <sup>16</sup> at the anode was reported, which results in irreversible sulfur loss and partially accounts for the declining discharge capacity.

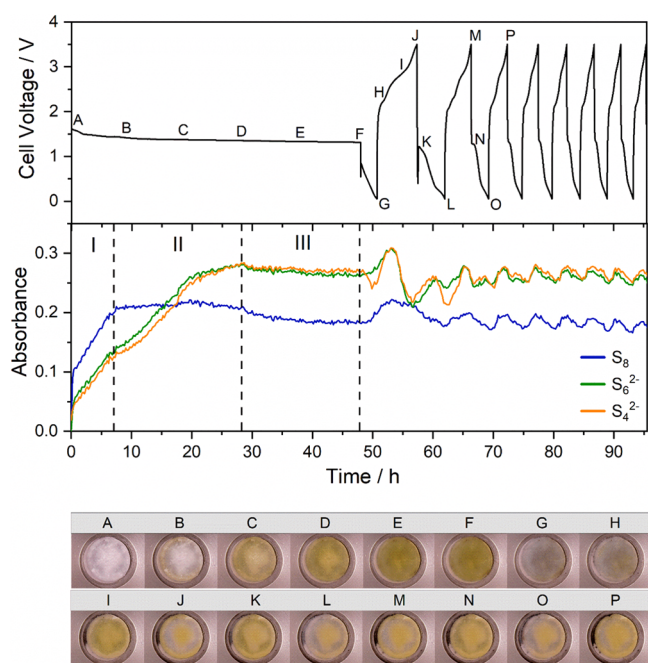


**Figure 8.** Voltage profile, absorbance and images of operando optical cells during 48 h OCV and subsequent cycling at C/20 comprising a 0.2 M  $\text{Mg}[\text{B}(\text{hfp})_4]_2/\text{G4}$  electrolyte and a S/KB/CMC-SBR (50/40/10 wt %) cathode. Three stages can be identified: (I) an initial rise in sulfur species concentration, (II) the ongoing reduction of sulfur to polysulfides, and (III) an equilibrium in sulfur species concentration.

With proceeding cycling, the differences in charge overpotential between the cathodes become negligible (Figure 7, cycle 5). This points to the additional reaction sites being covered by precipitated and (partially) inactive magnesium sulfide. This correlates perfectly with the decreasing charge-cutoff decay in  $\text{S}_4^{2-}/\text{S}_6^{2-}$  concentration with proceeding cycling (Figure S13). During discharge, the cathodes hardly differ in both potential and capacity gain with the additive-free cathode even providing slightly more capacity in the lower discharge plateau. Accompanied overpotentials of this rather steep “plateau” suggest sluggish kinetics, which evidently cannot be enhanced by increasing the conductive surface area. In general, the overpotentials of the solid–liquid reaction in the first discharge and charge plateau decrease with cycling from 1.2/1.3 to 1.5 V and from 2.2/2.3 to 2.1 V. In contrast, the overpotentials of the liquid–solid reaction in the second discharge and charge plateau increase with cycling from 0.6 to approximately 0.5 V and from 2.45 to 2.6 V, respectively, both pointing to the fact that magnesium sulfide and sulfur precipitation takes place on outer carbon surfaces rather than in the porous matrix. This facilitates the dissolution of solids due to the larger number of electrolyte molecules in their vicinity but, in the subsequent reaction, leads to a faster blocking of the conductive surface area by precipitates.

## SELF-DISCHARGE

Besides the galvanostatic cycling, the self-discharge was surveyed with an initial 48 h OCV period after cell assembly and prior to cycling. The voltage curve and the corresponding absorbance of the specific sulfur species are plotted in Figure 8.

Therein, the OCV period can be divided into three stages:

- (I) In the initial hours, the potential drops from 1.6 to 1.4 V and an increase of the  $\text{S}_8$  concentration is observed. In the same time, the concentrations of  $\text{S}_6^{2-}$  and  $\text{S}_4^{2-}$  rise due to the stepwise non-faradaic reduction of  $\text{S}_8$  to  $\text{S}_8^{2-}$  at the anode surface and further reaction to  $\text{S}_6^{2-}$  and  $\text{S}_4^{2-}$  electrochemically (eqs 2 and 3) or chemically (eqs 4 and 5).
- (II) After approximately 7 h OCV, the  $\text{S}_8$  concentration becomes constant, which suggests the solubility limit of the sulfur species in the electrolyte is reached. In pure G4, an  $\text{S}_8$  solubility limit of 7.5 mM is reported,<sup>29</sup> which is similar to those of other glymes (G1: 10 mM;<sup>30</sup> G2: 7.0 mM<sup>29</sup>). In electrolyte systems, the sulfur solubility is further reduced with increasing salt concentration as the amount of residual solvent molecules for coordination of sulfur species is minimized (0.1 M LiTFSI/G1 (9 mM), 1 M LiTFSI/G1 (4 mM)<sup>30</sup>). Considering the sulfur loading of 1 mg/cm<sup>2</sup>, i.e., 8.83  $\mu\text{mol}$  of sulfur in the cathode, and the applied electrolyte volume of 65  $\mu\text{L}$ , a maximum concentration of 17 mM  $\text{S}_8$  results. Therefore, the solubility limit should indeed be reached with sulfur still being partially present in the cathode. This is backed by the fact that the  $\text{S}_6^{2-}$  and  $\text{S}_4^{2-}$  concentrations concurrently rise via ongoing sulfur reduction at the anode to cause a yellowish coloration of the separator. Moreover, this also confirms that polysulfides are more soluble than sulfur,<sup>31</sup> leading to S-supersaturated electrolyte solutions in cycled cells.<sup>30</sup>
- (III) In the third stage, the concentrations of  $\text{S}_6^{2-}$  and  $\text{S}_4^{2-}$  become constant, while the  $\text{S}_8$  concentration slightly declines. This indicates the polysulfide solubility limit being reached, which further diminishes the sulfur concentration in solution.  $\text{S}_6^{2-}$  and  $\text{S}_4^{2-}$  appear to be rather stable in solution and neither disproportionation (eq 9/10) nor precipitation was observed. After 40 h OCV, the sulfur concentration becomes constant and an equilibrium of all sulfur species in solution is reached. Considering the missing first plateau in the subsequent discharge, it is concluded that there is no accessible  $\text{S}_8$  left in the cathode. A complete washout of sulfur from the cathode implies, that the porous carbon network is not capable of retaining any sulfur molecule, which is surprising as sulfur is in fact incorporated into the available pores (Table S3). However, because the main sulfur content is lost, the approach of mechanical intrusion of sulfur into the carbon matrix or the porous network of Ketjenblack itself seems unsuitable for sulfur retention.<sup>32</sup> As expected, cathodes with C45-additive exhibit a similar self-discharge behavior (Figure S14) as C45 does not provide tailored pore sizes to incorporate sulfur. In general, the quasi-solid-state concept—known to retain sulfur species in microporous carbons such as aerogels in the lithium–sulfur system<sup>33</sup>—might not be applicable for magnesium cells as it relies on the solid-state diffusion of cations and the  $\text{Mg}^{2+}$  diffusion is rather sluggish. A promising alternative strategy might be covalently bound sulfur in polymer chains (e.g., SPAN<sup>34</sup>).

Comparing identical cells during 48 h OCV reveals that the qualitative potential trend is reproducible (Figure S16). However, apart from the necessity of Mg metal (Figure S15) and the obvious influence of the sulfur retention capability of

the cathode, the electrolyte plays a crucial role in the context of self-discharge. Impurities (e.g., residual reactants or water) might result in an altered SEI formation due to non-faradaic reduction and therefore varied anode surface area to reduce sulfur species. Thus—as depicted in Figure S16—significant potential differences arise after cell assembly between different electrolyte batches (up to 0.5 V) but also between a single batch after 48 h OCV (up to 0.1 V).

As reported in our previous study,<sup>35</sup> the main parameters for self-discharge are (i) the mobility, solubility and dissolution kinetics of sulfur species and (ii) the kinetics of the side reactions on the Mg surface. Strategies to counteract the self-discharge by altering the dissolved sulfur species or their dissolution behavior increases ohmic losses and decreases the rate capability, respectively. This was investigated by a decrease in temperature, which indeed minimizes the sulfur loss, but also provokes a tremendous overpotential in the second discharge plateau.<sup>20</sup> The same is true when considering lean-electrolyte conditions to have less sulfur present in the liquid phase, because solid-phase kinetics are rather sluggish. The so-called solvent-in-salt approach applying a high concentrated electrolyte is reasonable due to lower  $S_8$  and  $MgS_x$  solubility,<sup>31</sup> however, sulfur dissolution might still occur, leading to electrolyte salt precipitation.<sup>15</sup> Therefore, the most promising approach is the prevention of sulfur reduction at the anode by an artificial SEI as this is not detrimental for the sulfur redox reactions at the cathode and additionally suppresses ongoing SEI growth. To mitigate the active material loss, an additional ion-selective separator coating toward the cathode side is reasonable.

Despite severe self-discharge, it was possible to cycle the cell after 48 h at OCV—albeit with reduced capacity compared to a cell rested for 1 h at OCV. Interestingly, the trend during charging with a significant decline in  $S_4^{2-}$ ,  $S_6^{2-}$ , and even  $S_8$  concentration (Figure 8J) rather follows the C45-cathode (Figure 4) than the identical cell with only 1 h OCV (Figure S7). This is probably due to the complete sulfur dissolution from the cathode during 48 h OCV and the Ketjenblack matrix again featuring a large surface area (Table S3), while exhibiting an even higher conductivity than C45 (5.471 vs 1.772 S/cm, Table S2). This effect is declining with proceeding cycling, again indicating the blocking of reaction sites by precipitates within the cathode matrix.

This study set out to analyze the magnesium polysulfide dissolution behavior in glyme-based electrolytes during cycling and rest at OCV. By applying operando UV/vis spectroscopy,  $S_8$ ,  $S_6^{2-}$ , and  $S_4^{2-}$  were identified as present species in the electrolyte, while  $S_8^{2-}$  and  $S_3^{•-}$  were not detected. During galvanostatic cycling,  $S_6^{2-}$  and  $S_4^{2-}$  are formed, diffuse in the electrolyte, and cause a bright yellow coloration of the electrolyte and separator. While there is a strong driving force for them to diffuse back to the cathode side during discharge, the electrolyte still exhibits a high sulfur species concentration after charge indicating incomplete reoxidation and active material loss. Conductive cathode additives such as carbon black (C45) or TiN can be beneficial by introducing additional reaction sites that enhance the reoxidation, leading to a decreased overpotential during charge and declining  $S_4^{2-}$  concentration toward charge-cutoff potential.

During extended rest at OCV, severe self-discharge takes places, which can be divided into three stages: (I)  $S_8$  is dissolved in the electrolyte and reduced at the anode to  $S_6^{2-}$  and  $S_4^{2-}$ , (II) the electrolyte becomes  $S_8$ -saturated, and the

$S_6^{2-}/S_4^{2-}$  concentration steadily increases, and (III) the  $S_8/S_6^{2-}/S_4^{2-}$  concentration in the electrolyte reaches an equilibrium. Neither disproportionation nor precipitation was observed, and the cell was cyclable afterward—albeit with reduced capacity gain. To mitigate self-discharge while not impairing redox kinetics, the most promising approach is the prevention of sulfur reduction at the anode by an artificial SEI.

## EXPERIMENTAL METHODS

For the cathode preparation, sulfur (99.5%, Alfa Aesar) and Ketjenblack EC 600-JD (Akzo Nobel) were ball-milled in 5/4 mass ratio, subsequently mixed with aqueous CMC (Walocel CRT 2000 PA, Dow Wolff) and SBR solution (JSR TRD 102A, JSR Micro), and coated on carbon-coated aluminum foil to result in a 50/40/10 wt % S/KB/CMC-SBR (1/2 CMC/SBR) cathode composition. In the case of utilizing additives, 10 wt % Super C45 (Imerys Graphite & Carbon) or TiN (97%, Chempur) were included in the slurry and a composition of 44.4/35.6/10/10 wt % S/KB/additive/CMC-SBR results. All cathodes exhibit a sulfur loading of approximately 1.0 mg/cm<sup>2</sup>. Ring-shaped pellets of magnesium powder (99.8%, 325 mesh, Alfa Aesar)—pressed and handled under argon atmosphere—were utilized as anodes.<sup>36</sup> 0.2 M  $Mg[B(hfp)_4]_2$  in tetraethylene glycol dimethyl ether (G4, tetraglyme, 99%, <10 ppm of H<sub>2</sub>O, Acros Organics) was applied as electrolyte.<sup>18</sup>

Operando measurements during galvanostatic cycling at C/20 with initial 1 and 48 h rest at OCV were performed in ECC-Opto-Std cells (EL-CELL) using a 6 mm sulfur cathode, 14/8 mm Mg pellet ring, two glass fiber separators (Whatman GF/C), and 65  $\mu$ L of electrolyte. The cell assembly was carried out in an argon-filled glovebox (O<sub>2</sub> and H<sub>2</sub>O < 1 ppm) with the cell components being thoroughly dried beforehand. Operando reflection UV/vis spectra and separator images were collected using a Maya2000Pro spectrometer (Ocean Insight) and an USB camera module (USB 2.0 UVC PC), respectively.

## ASSOCIATED CONTENT

### Supporting Information

The Supporting Information is available free of charge at <https://pubs.acs.org/doi/10.1021/acsenerylett.1c02152>.

Details about the electrode and electrolyte preparation as well as the optical cell and operando UV/vis spectroscopy/microscopy setup; sulfur species absorbance in various solvents from previous reports; SEM and EDX analysis of the different cathodes; additional galvanostatic cycling and self-discharge experiments (PDF)

## AUTHOR INFORMATION

### Corresponding Author

Joachim Häcker – Institute of Engineering Thermodynamics, German Aerospace Center (DLR), 70569 Stuttgart, Germany; [orcid.org/0000-0003-2031-9898](https://orcid.org/0000-0003-2031-9898); Email: [joachim.haecker@dlr.de](mailto:joachim.haecker@dlr.de)

### Authors

Duc Hien Nguyen – Institute of Engineering Thermodynamics, German Aerospace Center (DLR), 70569 Stuttgart, Germany; Department of Nanochemistry, Max-Planck-Institute for Solid State Research, 70569 Stuttgart, Germany; [orcid.org/0000-0002-3442-1159](https://orcid.org/0000-0002-3442-1159)

Tobias Rommel – Institute of Engineering Thermodynamics, German Aerospace Center (DLR), 70569 Stuttgart, Germany; [orcid.org/0000-0001-8945-4444](https://orcid.org/0000-0001-8945-4444)

Zhirong Zhao-Karger – Helmholtz Institute Ulm (HIU) Electrochemical Energy Storage, 89081 Ulm, Germany; [orcid.org/0000-0002-7233-9818](https://orcid.org/0000-0002-7233-9818)

Norbert Wagner – Institute of Engineering Thermodynamics, German Aerospace Center (DLR), 70569 Stuttgart, Germany

K. Andreas Friedrich – Institute of Engineering Thermodynamics, German Aerospace Center (DLR), 70569 Stuttgart, Germany; Institute of Building Energetics, Thermal Engineering and Energy Storage (IGTE), University of Stuttgart, 70569 Stuttgart, Germany

Complete contact information is available at:

<https://pubs.acs.org/10.1021/acsenergylett.1c02152>

## Notes

The authors declare no competing financial interest.

## ACKNOWLEDGMENTS

This work is financially supported by the Federal Ministry for Education and Research of Germany (Bundesministerium für Bildung und Forschung, BMBF) and the European Union within the projects MagSiMal (03XP0208) and E-MAGIC (824066), respectively. We also express our gratitude to Pia Lange and Ina Plock for sample preparation and characterization, as well as EL-CELL and Ocean Insight for providing essential test equipment.

## REFERENCES

- (1) Bonnicksen, P.; Muldoon, J. A Trip to Oz and a Peak Behind the Curtain of Magnesium Batteries. *Adv. Funct. Mater.* **2020**, *30* (21), 1910510.
- (2) Li, M.; Lu, J.; Ji, X.; Li, Y.; Shao, Y.; Chen, Z.; Zhong, C.; Amine, K. Design strategies for nonaqueous multivalent-ion and monovalent-ion battery anodes. *Nature Reviews Materials* **2020**, *5* (4), 276–294.
- (3) Yu, X.; Manthiram, A. Performance Enhancement and Mechanistic Studies of Magnesium-Sulfur Cells with an Advanced Cathode Structure. *ACS Energy Letters* **2016**, *1* (2), 431–437.
- (4) Robba, A.; Vizintin, A.; Bitenc, J.; Mali, G.; Arcon, I.; Kavcic, M.; Zitnik, M.; Bucar, K.; Aquilanti, G.; Martineau-Corcoss, C.; Randon-Vitanova, A.; Dominko, R. A Mechanistic Study of Magnesium Sulfur Batteries. *Chem. Mater.* **2017**, *29*, 9555–9564.
- (5) Nakayama, Y.; Matsumoto, R.; Kumagai, K.; Mori, D.; Mizuno, Y.; Hosoi, S.; Kamiguchi, K.; Koshitani, N.; Inaba, Y.; Kudo, Y.; Kawasaki, H.; Miller, E. C.; Weker, J. N.; Toney, M. F. Zinc Blende Magnesium Sulfide in Rechargeable Magnesium-Sulfur Batteries. *Chem. Mater.* **2018**, *30* (18), 6318–6324.
- (6) Barchasz, C.; Molton, F.; Duboc, C.; Leprêtre, J.-C.; Patoux, S.; Alloin, F. Lithium/Sulfur Cell Discharge Mechanism: An Original Approach for Intermediate Species Identification. *Anal. Chem.* **2012**, *84* (9), 3973–3980.
- (7) Cañas, N. A.; Fronczek, D. N.; Wagner, N.; Latz, A.; Friedrich, K. A. Experimental and Theoretical Analysis of Products and Reaction Intermediates of Lithium–Sulfur Batteries. *J. Phys. Chem. C* **2014**, *118* (23), 12106–12114.
- (8) Marceau, H.; Kim, C.-S.; Paolella, A.; Ladouceur, S.; Lagacé, M.; Chaker, M.; Vijh, A.; Guerfi, A.; Julien, C. M.; Mauger, A.; Armand, M.; Hovington, P.; Zaghbi, K. In operando scanning electron microscopy and ultraviolet–visible spectroscopy studies of lithium/sulfur cells using all solid-state polymer electrolyte. *J. Power Sources* **2016**, *319*, 247–254.
- (9) Zou, Q.; Lu, Y.-C. Solvent-Dictated Lithium Sulfur Redox Reactions: An Operando UV–vis Spectroscopic Study. *J. Phys. Chem. Lett.* **2016**, *7* (8), 1518–1525.
- (10) Patel, M. U. M.; Demir-Cakan, R.; Morcrette, M.; Tarascon, J.-M.; Gaberscek, M.; Dominko, R. Li-S Battery Analyzed by UV/Vis in Operando Mode. *ChemSusChem* **2013**, *6* (7), 1177–1181.
- (11) Patel, M. U. M.; Dominko, R. Application of In Operando UV/Vis Spectroscopy in Lithium–Sulfur Batteries. *ChemSusChem* **2014**, *7* (8), 2167–2175.
- (12) Zhao-Karger, Z.; Zhao, X.; Wang, D.; Diemant, T.; Behm, R. J.; Fichtner, M. Performance Improvement of Magnesium Sulfur Batteries with Modified Non-Nucleophilic Electrolytes. *Adv. Energy Mater.* **2015**, *5* (3), 1401155.
- (13) Bieker, G.; Wellmann, J.; Kolek, M.; Jalkanen, K.; Winter, M.; Bieker, P. Influence of cations in lithium and magnesium polysulfide solutions: dependence of the solvent chemistry. *Phys. Chem. Chem. Phys.* **2017**, *19*, 11152–11162.
- (14) Bieker, G.; Diddens, D.; Kolek, M.; Borodin, O.; Winter, M.; Bieker, P.; Jalkanen, K. Cation-Dependent Electrochemistry of Polysulfides in Lithium and Magnesium Electrolyte Solutions. *J. Phys. Chem. C* **2018**, *122* (38), 21770–21783.
- (15) Drvarič Talian, S.; Vizintin, A.; Bitenc, J.; Aquilanti, G.; Randon-Vitanova, A.; Gabersček, M.; Dominko, R. Magnesium Polysulfides: Synthesis, Disproportionation, and Impedance Response in Symmetrical Carbon Electrode Cells. *ChemElectroChem* **2021**, *8* (6), 1062–1069.
- (16) Ford, H. O.; Doyle, E.; He, P.; Boggess, W. C.; Oliver, A. G.; Wu, T.; Sterbinsky, G. E.; Schaefer, J. Self-discharge of magnesium–sulfur batteries leads to active material loss and poor shelf life. *Energy Environ. Sci.* **2021**, *14* (2), 890–899.
- (17) Rauh, R. D.; Shuker, F. S.; Marston, J. M.; Brummer, S. B. Formation of lithium polysulfides in aprotic media. *J. Inorg. Nucl. Chem.* **1977**, *39* (10), 1761–1766.
- (18) Zhao-Karger, Z.; Liu, R.; Dai, W.; Li, Z.; Diemant, T.; Vinayan, B. P.; Bonatto Minella, C.; Yu, X.; Manthiram, A.; Behm, R. J.; Ruben, M.; Fichtner, M. Toward Highly Reversible Magnesium–Sulfur Batteries with Efficient and Practical Mg[B(hfip)4]2 Electrolyte. *ACS Energy Letters* **2018**, *3* (8), 2005–2013.
- (19) Dev, S.; Ramli, E.; Rauchfuss, T. B.; Wilson, S. R. Synthesis and structure of [M(N-methylimidazole)6]S8 (M = manganese, iron, nickel, magnesium). Polysulfide salts prepared by the reaction N-methylimidazole + metal powder + sulfur. *Inorg. Chem.* **1991**, *30* (11), 2514–2519.
- (20) Häcker, J.; Danner, C.; Sievert, B.; Biswas, I.; Zhao-Karger, Z.; Wagner, N.; Friedrich, K. A. Investigation of Magnesium–Sulfur Batteries using Electrochemical Impedance Spectroscopy. *Electrochim. Acta* **2020**, *338*, 135787.
- (21) Cui, Z.; Zu, C.; Zhou, W.; Manthiram, A.; Goodenough, J. B. Mesoporous Titanium Nitride-Enabled Highly Stable Lithium-Sulfur Batteries. *Adv. Mater.* **2016**, *28* (32), 6926–31.
- (22) Mosavati, N.; Chitturi, V. R.; Salley, S. O.; Ng, K. Y. S. Nanostructured titanium nitride as a novel cathode for high performance lithium/dissolved polysulfide batteries. *J. Power Sources* **2016**, *321*, 87–93.
- (23) Deng, D.-R.; An, T.-H.; Li, Y.-J.; Wu, Q.-H.; Zheng, M.-S.; Dong, Q.-F. Hollow porous titanium nitride tubes as a cathode electrode for extremely stable Li–S batteries. *J. Mater. Chem. A* **2016**, *4* (41), 16184–16190.
- (24) Hao, Z.; Yuan, L.; Chen, C.; Xiang, J.; Li, Y.; Huang, Z.; Hu, P.; Huang, Y. TiN as a simple and efficient polysulfide immobilizer for lithium–sulfur batteries. *J. Mater. Chem. A* **2016**, *4* (45), 17711–17717.
- (25) Jeong, T.-G.; Choi, D. S.; Song, H.; Choi, J.; Park, S.-A.; Oh, S. H.; Kim, H.; Jung, Y.; Kim, Y.-T. Heterogeneous Catalysis for Lithium–Sulfur Batteries: Enhanced Rate Performance by Promoting Polysulfide Fragmentations. *ACS Energy Letters* **2017**, *2* (2), 327–333.
- (26) Hussain, S.; Yang, X.; Aslam, M. K.; Shaheen, A.; Javed, M. S.; Aslam, N.; Aslam, B.; Liu, G.; Qiao, G. Robust TiN nanoparticles

polysulfide anchor for Li–S storage and diffusion pathways using first principle calculations. *Chem. Eng. J.* **2020**, *391*, 123595.

(27) Vinayan, B. P.; Zhao-Karger, Z.; Diemant, T.; Chakravadhanula, V. S. K.; Schwarzburger, N. I.; Cambaz, M. A.; Behm, R. J.; Kubel, C.; Fichtner, M. Performance study of magnesium-sulfur battery using a graphene based sulfur composite cathode electrode and a non-nucleophilic Mg electrolyte. *Nanoscale* **2016**, *8*, 3296–3306.

(28) Xu, Y.; Ye, Y.; Zhao, S.; Feng, J.; Li, J.; Chen, H.; Yang, A.; Shi, F.; Jia, L.; Wu, Y.; Yu, X.; Glans-Suzuki, P.-A.; Cui, Y.; Guo, J.; Zhang, Y. In Situ X-ray Absorption Spectroscopic Investigation of the Capacity Degradation Mechanism in Mg/S Batteries. *Nano Lett.* **2019**, *19* (5), 2928–2934.

(29) Sciamanna, S. F.; Lynn, S. Sulfur Solubility in Pure and Mixed Organic Solvents. *Ind. Eng. Chem. Res.* **1988**, *27* (3), 485–491.

(30) Zheng, D.; Zhang, X.; Li, C.; McKinnon, M. E.; Sadok, R. G.; Qu, D.; Yu, X.; Lee, H.-S.; Yang, X.-Q.; Qu, D. Quantitative Chromatographic Determination of Dissolved Elemental Sulfur in the Non-Aqueous Electrolyte for Lithium-Sulfur Batteries. *J. Electrochem. Soc.* **2015**, *162* (1), A203–A206.

(31) Gao, T.; Hou, S.; Wang, F.; Ma, Z.; Li, X.; Xu, K.; Wang, C. Reversible S<sub>0</sub>/MgS<sub>x</sub> Redox Chemistry in a MgTFSI<sub>2</sub>/MgCl<sub>2</sub>/DME Electrolyte for Rechargeable Mg/S Batteries. *Angew. Chem., Int. Ed.* **2017**, *56* (43), 13526–13530.

(32) Richter, R.; Häcker, J.; Zhao-Karger, Z.; Danner, T.; Wagner, N.; Fichtner, M.; Friedrich, K. A.; Latz, A. Degradation Effects in Metal–Sulfur Batteries. *ACS Applied Energy Materials* **2021**, *4* (3), 2365–2376.

(33) Nojabae, M.; Sievert, B.; Schwan, M.; Schettler, J.; Warth, F.; Wagner, N.; Milow, B.; Friedrich, K. A. Ultramicroporous Carbon Aerogel Encapsulating Sulfur as Cathode for Lithium-Sulfur Batteries. *J. Mater. Chem. A* **2021**, *9*, 6508–6519.

(34) Wang, P.; Kappler, J.; Sievert, B.; Häcker, J.; Küster, K.; Starke, U.; Ziegler, F.; Buchmeiser, M. R. Characteristics of magnesium-sulfur batteries based on a sulfurized poly(acrylonitrile) composite and a fluorinated electrolyte. *Electrochim. Acta* **2020**, *361*, 137024.

(35) Richter, R.; Häcker, J.; Zhao-Karger, Z.; Danner, T.; Wagner, N.; Fichtner, M.; Friedrich, K. A.; Latz, A. Insights into Self-Discharge of Lithium– and Magnesium–Sulfur Batteries. *ACS Applied Energy Materials* **2020**, *3* (9), 8457–8474.

(36) Sievert, B.; Häcker, J.; Bienen, F.; Wagner, N.; Friedrich, K. A. Magnesium Sulfur Battery with a New Magnesium Powder Anode. *ECS Trans.* **2017**, *77* (11), 413.

**JACS Au**  
AN OPEN ACCESS JOURNAL OF THE AMERICAN CHEMICAL SOCIETY

Editor-in-Chief  
**Prof. Christopher W. Jones**  
Georgia Institute of Technology, USA

**Open for Submissions**

pubs.acs.org/jacsau ACS Publications  
Most Trusted. Most Cited. Most Read.